Experimental analysis of the temperature and concentration profiles in a salinity gradient solar pond with, and without a liquid cover to suppress evaporation

Asaad H. Sayer*[1, 2]

a.h.sayer@surrey.ac.uk

* Corresponding author. Tel +44 1483686562

Hazim Al-Hussaini[1]

h.al-hussaini@surrey.ac.uk

Alasdair N. Campbell[1]

a.n.campbell@surrey.ac.uk

[1]Department of Chemical and Process Engineering, Faculty of Engineering and Physical Sciences, University of Surrey GU2 7XH, UK

[2]University of Thi-Qar, College of Science, Chemistry Department, Thi-Qar, Iraq

alimmz5@yahoo.com

Abstract

Solar ponds offer an effective way to collect and store incident solar radiation, making them an attractive alternative to photovoltaic systems for applications which require low-grade heat to operate. If these ponds are to be implemented successfully, then a more complete understanding of the mechanisms and phenomena governing their behaviour is required. Evaporation has been shown previously to be the dominant mode of heat loss from the pond surface, and the fresh water that would need to be added to maintain the pond's inventory could potentially add significantly to operating costs. To this end, an experimental unit was constructed to examine and observe the behaviour of a salinity gradient solar pond (SGSP) before and after covering the pond with a thin layer (0.5 cm) of paraffin, with the aim of eliminating evaporation. The unit was run for 71 days in Nasiriyah, Iraq. This is the first study to attempt to completely eliminate the harmful effects of evaporation on solar pond performance using a liquid layer. The layer successfully eliminated the significant evaporation observed from the uncovered pond and crucially, while the salinity gradient through the non-convective zone remained substantially intact over the course of the study, the temperature profile became approximately uniform throughout the entire pond after about 50 days. This behaviour has significant implications for the construction of the pond, as it may mean that if evaporation can be largely suppressed, the salinity gradient may not be necessary for the pond to capture and efficiently store heat. Furthermore, the effects on evaporation of different climatic factors such as relative humidity, wind speed, ambient temperature and solar radiation

were considered by analysing data measured on-site and longer-term meteorological data. The results showed that ambient temperature, solar radiation and humidity have a significant correlation with the evaporation rate; and their impact varies seasonally. A more comprehensive multiple regression analysis showed that ambient temperature has the highest impact on evaporation, while the effect of the incident solar radiation is insignificant. Such insights are vital in the design and siting of solar ponds, and can be used to minimise evaporative losses.

Nomenclature

k	Number of variables
n	Number of observations
$AdjR^2$	Adjusted standard deviation
R^2	Standard deviation
R	Correlation coefficient

Abbreviation

LCZ	Lower convective zone
NCZ	Non-convective zone
SGSP	Salinity gradient solar pond
UCZ	Upper convective zone

1. Introduction

The increase in the demand for clean and sustainable energy is encouraging researchers and scientific centres around the world to focus on finding new means of capturing, storing and exploiting renewable energy sources. Solar ponds are a means to both capture and, remarkably, store the incoming solar radiation in the form of low-grade heat. There are several possible configurations for a solar pond, but of these, the salinity gradient solar pond (SGSP) is the most commonly investigated and constructed type. A SGSP integrates the collection and storage of solar energy and can be used throughout the year, irrespective of time and season (Karakilcik et al., 2006). It is a relatively simple and low-cost technology which nevertheless possesses a substantial thermal mass. It can also be constructed from readily available and low-priced raw materials. Srinivasan (1993) pointed out that the cost of a SGSP is much less than that of an equivalent flat plate collector. On the other hand, he also implied that the initial cost of the SGSP is high and strongly depends on the site of the pond. Nevertheless, availability of solar

irradiance at the location of interest should be considered for conducting feasibility studies. There are several types of data sets providing solar irradiance data and solar data estimation methods studied in several research works (Jahani et al., 2015).

The SGSP can supply thermal energy to a wide variety of applications that necessitate only low-grade heat to run. Examples include providing heat for buildings, power generation (utilising an organic Rankine cycle), water desalination, greenhouse heating, biogas production, process heating, agricultural crop drying and aquaculture such as for growing warm water fish and shrimps (Ruskowitz et al., 2014; Hull et al., 1988; Alrowaished et al., 2013; El-Sebaii et al., 2011; Date and Akbarzadeh, 2013; Liu et al., 2013; Caruso and Naviglio, 1999; Dehghan et al., 2013; Kurt et al., 2000; Sakhrieh and Al-Salaymeh, 2013; Abdullah et al., 2015; Abbassi Monjezi and Campbell, 2016; and Abbassi Monjezi and Campbell, 2017a). Using SGSPs in such a diverse array of applications is potentially economically beneficial and environmentally friendly. It has been recommended that future efforts should focus on the development of thermal energy storage with low capital and maintenance costs (Antipova et al., 2013; Gude, 2015; Suarez et al., 2015; Salata and Coppi, 2014; Gude et al., 2012; and Ghaffour et al., 2014). The SGSP fits this bill perfectly. It is, however, distinctly possible that if SGSPs are coupled to desalination technologies, a very significant proportion of the water produced would be required to replace the pond water lost to evaporation, rendering the ponds uneconomic. It is therefore of vital importance that this process is understood fully, and that the effect of eliminating evaporation is studied empirically. Moreover, the possibility of increasing the light absorbance of the LCZ and consequently its temperature using nanoparticles can also be considered for future work. Rahimi et al. (2015) studied the preparation and characterisation of photocatalytic nanoparticles. Their research can be extended further to examine the benefits of using nanoparticles in the SGSP.

A significant number of studies has focused on using SGSPs as an energy source for applications beyond desalination that require only low-grade heat (Ranjan and Kaushik, 2014; Zaragoza et al., 2014; Bozkurt and Karakilcik, 2012; Abdullah and Lindsay, 2016; Ziapour et al., 2016; and Abbassi Monjezi and Campbell, 2017b). It is vital that if the potential of these applications is to be realised, the fundamental issues with solar pond performance, efficiency and cost are tackled. To this end, this study seeks to demonstrate the effect on pond performance of completely suppressing heat and mass losses by evaporation. These losses are one of the main barriers to the successful implementation of solar ponds (Ruskowitz et al., 2014; Sayer et al., 2016).

1.1 Salinity gradient solar ponds

A salinity gradient solar pond is a body of water with a depth of between 2 and 5 m, which has variable salt concentration to suppress convection (Leblanc et al., 2011). It is comprised of three distinct zones: the surface zone or the upper convective zone (UCZ), the middle zone or non-convective zone (NCZ) and the lower convective zone (LCZ) (Jaefarzadeh, 2004). The UCZ is approximately homogenous, and is a relatively cold layer of freshwater or low salinity brine. The NCZ has a salinity gradient, i.e. the salinity increases from the top to the bottom of the layer. The bottom zone (LCZ) has a high salinity, usually close to saturation, and is designed to store the received solar radiation (Date and Akbarzadeh, 2013). Convective heat loss from the LCZ through the NCZ is suppressed due to the salinity gradient and the resultant density gradient, which suppresses natural convection in this layer. Heat loss therefore occurs by conduction only; the NCZ effectively works as an insulator. Torkmahalleh et al. (2017) examined the performance of a small SGSP in a Mediterranean climate for 10 months. They found that the temperature of the NCZ and LCZ depended on the ambient temperature and the incident solar radiation. Abdullah et al. (2016) constructed a SGSP with a surface area of 113 m^2 at Umm Al-Qura University, Saudi Arabia. Their work illustrates the technical viability of SGSP technology in the Middle East. However, a crucial barrier to the implementation of these seemingly simple ponds is the lack of information about their behaviour, and in particular the lack of empirical data from field trials, as the ponds have more often been studied theoretically, with little empirical validation. For example, Husain et al. (2012) investigated theoretically enhancing SGSP performance by judicious selection of the size of the NCZ. They concluded that the LCZ temperature could be increased by 20 °C when the optimum NCZ depth is chosen. However, their findings need to be proved experimentally. Dah et al. (2010) studied theoretically and experimentally the improvement in SGSP performance by extracting heat from the NCZ. This enhanced the efficiency of the pond, but also decreased the stability of the LCZ, which is crucial to the pond's functioning.

1. 2 Evaporation

Sayer et al. (2016) concluded that surface heat loss from a SGSP by evaporation was significant in comparison to losses by convection and radiation. Their theoretical results illustrated that preventing surface evaporation could significantly increase temperatures in the UCZ and LCZ. Ruskowitz et al. (2014) experimentally observed that when evaporation was decreased, there was an apparent increase in the LCZ temperature. They also concluded that the amount of heat lost to the atmosphere decreased, and there was a noticeable increase in the

NCZ temperature. Many other studies (Akbarzadeh et al., 2005; Tabor, 1980; Akbarzadeh and Ahmadi, 1979; Ali, 1989; Alagao et al., 1994; and Alagao, 1996) affirmed that evaporation and the depth of the underground water table had a significant effect on the performance of the SGSP. A shallow water table would increase the heat loss to the ground, but this could be tackled by insulating the base of the pond sufficiently. In contrast, a high evaporation rate would increase heat and water loss to the atmosphere, and preventing this might be more difficult. The reduction or elimination of surface evaporation would also potentially enable such ponds to operate in areas with water shortages, since the water required to replenish the UCZ is reduced.

Assouline et al. (2010) used non-transparent polypropylene sheets as an evaporation suppressor. The main aim of their study was to suppress evaporative losses, without taking into consideration the heat trapped in the pond. In such a scenario, any opaque floating material can be utilised to reduce or eliminate evaporative losses. However, for solar ponds, the use of opaque materials is not appropriate because the solar radiation penetrating the layers of water will be significantly attenuated and consequently the performance of the pond will decrease.

Ruskowitz et al. (2014) investigated the suppression of evaporative losses from a SGSP in the laboratory. Three methods were tested: the first using a continuous plastic cover, the second and third using floating element designs (discs and hemispheres). All the materials used were transparent. With the floating discs (the most efficient method), evaporation decreased by 47% and the LCZ temperature rose by 26%. It is important to note that this study was carried out in the laboratory using artificial light, thereby excluding the effect of climatic factors (incident solar radiation, relative humidity, ambient temperature and wind speed).

Assari et al. (2015) carried out a three-month experimental study in Dezful, Iran, from May to August 2012, considering the behaviour of different shapes of solar ponds covered by plastic glazing to prevent evaporation from the surface of the pond. Two shapes, rectangular and circular, with similar volumes, were examined. Two small ponds were used with a height and surface area of 0.63 m and 0.51 m^2 respectively. The results showed that evaporation decreased significantly and maximum temperatures reached 74 and 71 °C for the rectangular and circular ponds respectively. There is therefore a clear benefit to suppressing evaporation, but the method employed (i.e. covering with glazing) can only be used in a small pond.

The objective of this research was to study the suppression of evaporation from a SGSP using a thin layer of liquid paraffin, and to investigate the change in temperatures in the pond's zones. As such, this study provides the first data from proof-of-concept field trials in which evaporation has been completely suppressed using a liquid film. It highlights both the potential

benefits and challenges that result from using an immiscible non-volatile liquid covering and raises future research questions that would have to be addressed if such a solution were to be deployed at full scale. Paraffin was selected because it is transparent, highly immiscible with water and of lower density than water. The high boiling and low melting points (158 and -21 °C respectively) of the paraffin liquid enable it to be stable on the water's surface. To perform the study, a small experimental SGSP was constructed. A detailed explanation of the pond and its results are presented below.

1. Experimental work and materials

The experimental study was carried out over 71 days starting on 29 July 2015. A small SGSP with a surface area of 1 m^2, and a depth of 1 m (1 m^3 volume) was constructed in Nasiriyah in southern Iraq (Latitude: 31.05799°, Longitude: 46.25726°). The temperature in the pond was monitored during the day and night time. Moreover, the concentration variation with time was measured to observe the diffusion of salt (NaCl) throughout the pond's zones during the study. Concentration measurements were performed *ex-situ* by taking samples from the LCZ, NCZ and UCZ after 6, 12, 30 and 50 days of operation. The salt concentration in these samples was measured using a calibrated conductivity meter (HANNA HI2300, Romania), which can measure a range of concentrations from 0-400 g/l NaCl (accuracy ±1%). The experimental unit was a tank made of galvanized steel sheets of 1 mm thickness. The side walls and base of the tank were surrounded by a wooden frame of thickness 2 cm. In between these layers was a 6 cm layer of polystyrene which acted as an insulator, to reduce heat loss from the walls. The small pond was mounted on a closed wooden box of height 10 cm. Thus, the entirety of the pond was above ground. The wooden box's walls were 2 cm thick. Between these walls, an additional 6 cm layer of polystyrene was inserted to minimize heat loss to the ground. The inner sides of the pond were painted black, providing an anti-corrosion barrier and increasing the solar radiation absorptivity. Figure 1 shows the schematic of the experimental unit.

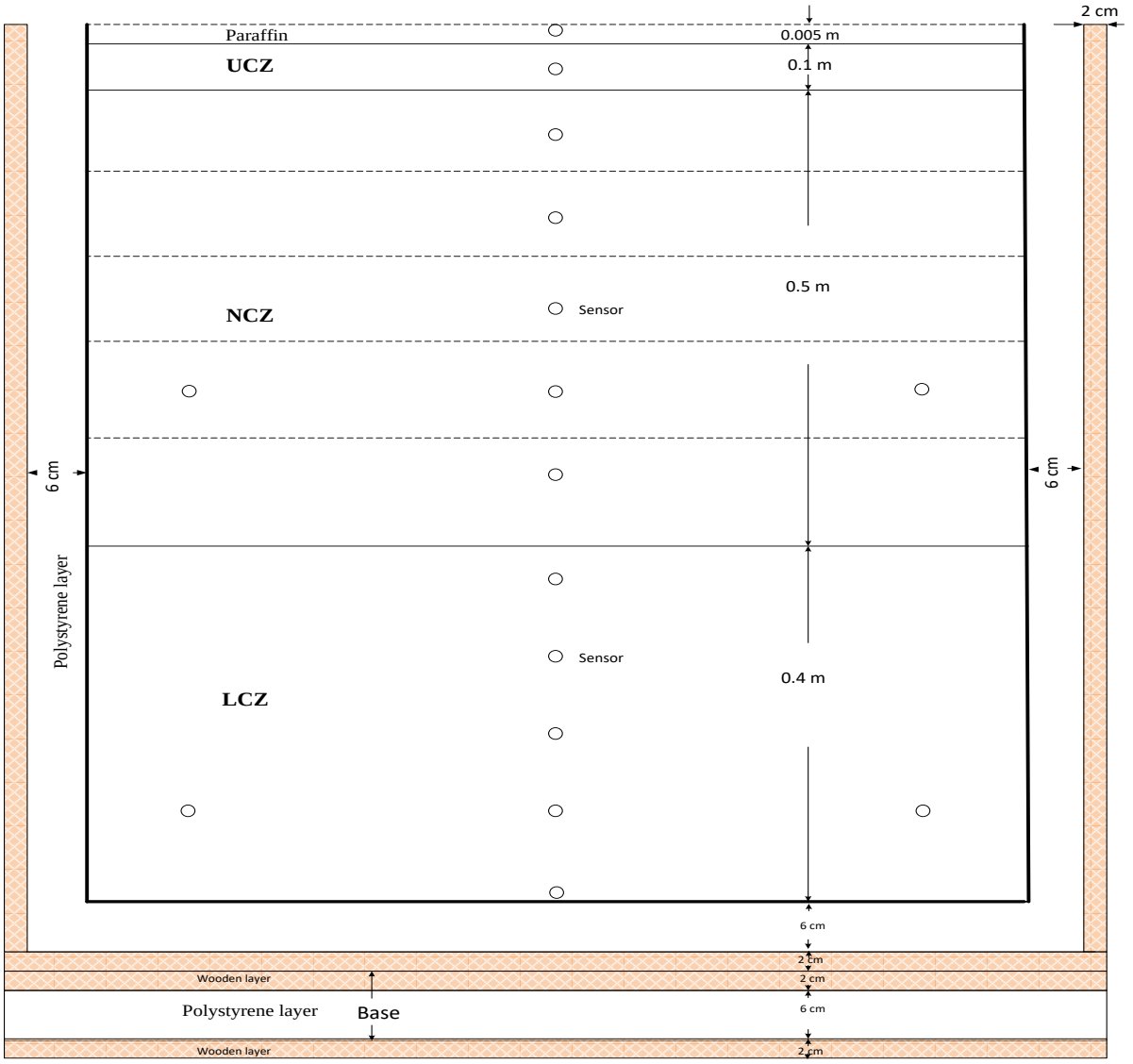

Figure 1: Schematic diagram showing cross-section of the experimental SGSP and distribution of the thermocouples monitoring the spatio-temporal evolution of the temperature field. The dashed horizontal lines in the NCZ show the layers used to construct the salinity gradient

The three layers of the SGSP – the UCZ, NCZ and LCZ - must be constructed carefully to ensure the correct salinity gradient is established. The methods used were similar to those used by Suarez et al. (2014) and Aizaz and Yousaf (2013). Firstly, to form the storage zone (LCZ), a solution with high salt (NaCl) concentration (0.25 kg/l) was prepared in a mixing tank and transferred to the experimental pond using a small pump; this forms the storage zone of the pond. The layer had a depth of 0.4 m.

The second layer to be added, the NCZ. It is considered critical to the operation of a SGSP (see e.g. Karakilcik et al., 2006; Karakilcik et al., 2013; and Velmurugan and Srithar, 2008). The layer is transparent, allowing the incident solar radiation to penetrate to the LCZ. It was

constructed by adding five 10 cm layers of salty water of decreasing concentration (and hence density) to the top of the LCZ, giving a total NCZ depth of 0.5 m. The solution for each layer, with successive concentrations of 0.2, 0.15, 0.1, 0.05 and 0.025 kg/l, was prepared separately in the mixing tank and pumped gently onto the surface of the previous layer. To minimise mixing between the layers, a small network of pipes with many small holes (of 0.5 mm diameter) was used at the end of the transfer pipe, to add the water to the pond with minimal momentum. To further reduce the momentum of the exiting water, the network of pipes was wrapped by a piece of perforated cloth. This technique, combined with the low flow rate (0.25 l / min) minimised any disturbance of the layers.

The final layer, the UCZ, had a thickness of 0.1 m and was created with fresh water. This layer requires continuous observation as it is open to the atmosphere. Its thickness and transparency can be affected by many factors, such as wind speed, rainfall and dust. After construction, the pond was exposed to natural solar radiation and other climatic factors.

After 12 days of heat collection, a paraffin layer with a thickness of 0.5 cm was added to the top of the UCZ. This 12-day period was chosen to ensure that the salinity and temperature gradients became established before the paraffin was added.

The experimental temperature distributions were measured using 16 calibrated K type thermocouples (LABFACILITY ZO-PFA-K-1 X 5, Great Britain). The uncertainty of the thermocouples in the experimental unit was tested by the calibration against boiling (100 °C) and melting (0 °C) water. The uncertainty was estimated to be ±3 °C.

As shown in Figure 1, the thermocouples were fixed along the vertical centre line of the pond, to measure the vertical temperature profiles of each zone (UCZ, NCZ, LCZ and the paraffin layer). Thermocouples were located, measuring from the bottom of the pond to the edge of the LCZ, at heights of 0, 0.05, 0.15, 0.25 and 0.35 m. Two further thermocouples were placed in the LCZ to monitor the temperature change in the horizontal direction. Seven sensors were placed in the NCZ at intervals of 10 cm. As with the LCZ, two additional thermocouples were placed at the bottom of the NCZ to measure the horizontal temperature distribution. For the UCZ, a single thermocouple was fixed in the centre of the layer to measure the temperature there. The last sensor was used to measure temperature in the paraffin layer.

All the thermocouples were connected to a control board with a multichannel digital reader by 2 m extension wires. The temperatures in all zones were measured during the day (2 p.m.) and night (2 a.m.).

To quantify the effect of weather conditions, a Gray Wolf IQ-610 (USA) was used to measure relative humidity and ambient temperature, and model AS-201 (USA) to measure wind speed above the water surface. The incident solar insolation was not measured.

3. Results and discussion

3.1 Evaporation

Evaporation levels were measured daily for the 12 days before the pond was covered, by reading the water level in the UCZ before and after fresh water had been injected into this layer to maintain the depth of the pond. It was observed that evaporation levels were high, reaching 21 l/m^2 day. The weather on these days was windy, hot and dry. The major factors which can influence evaporation significantly are humidity, ambient temperature, wind speed and incident solar radiation. Figure 2 shows the measurements of the evaporation rate, relative humidity and ambient temperature for the 12 days before the paraffin addition, when the surface of the UCZ was exposed to the atmosphere.

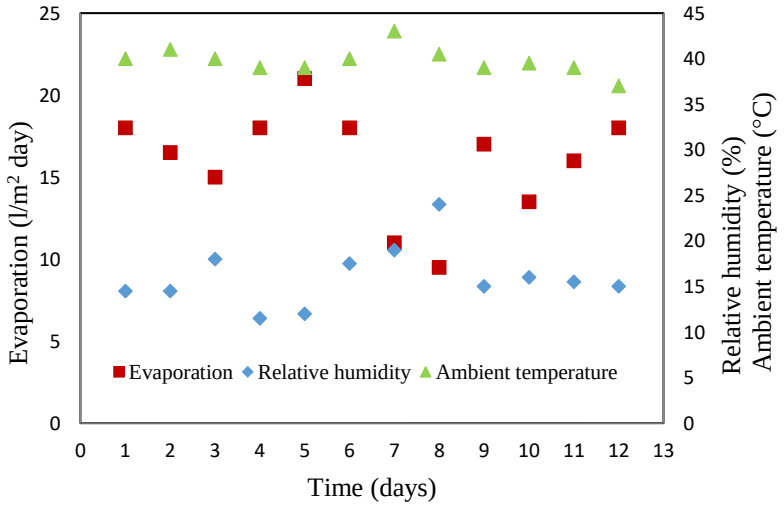

(a)

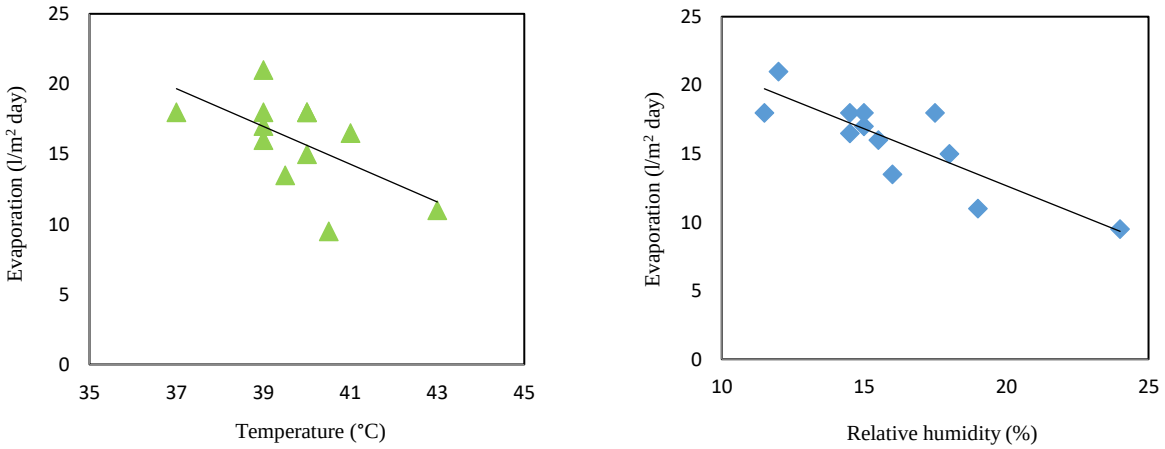

(b) (c)

Figure 2: (a) Daily average measurements of evaporation rate, relative humidity and the ambient temperature for the experimental pond for 12 days from 29/7-9/8/2015. (b) Scatter plot of daily evaporation rate versus average temperature. (c) Scatter plot of the evaporation rate versus average relative humidity.

Figure 2(a) illustrates that the ambient temperature had only a small impact on evaporation levels over the 12 days. The average temperature was relatively high and consistent at around 39-41 °C, whereas the evaporation rate shows significant scatter. However, it is evident from Figure 2(b) that for this 12-day period there is a weak negative correlation between the ambient temperature and evaporation rate. The correlation coefficient (R) of the ambient temperature with evaporation is -0.59, which indicates only a relatively moderate negative correlation.

From Figure 2(a), it appears that relative humidity has a significant effect on the evaporation rate. The results show that relative humidity and evaporation rate are negatively correlated. For example, on Day 3 there was a noticeable increase in relative humidity and an apparent decrease in evaporation. Similarly, on Days 5 and 8 when relative humidity decreased (Day 5), evaporation increased significantly; when it increased (Day 8), there was a substantial reduction in evaporation. Similar behaviour can be observed on other days. This makes intuitive sense, as the higher the humidity, the lower the driving force for mass transfer from the water to the air, and vice versa. Figure 2(c) also shows that there is a much stronger correlation between evaporation and relative humidity with R = - 0.85.

The effect of wind speed on the evaporation level is shown in Figure 3.

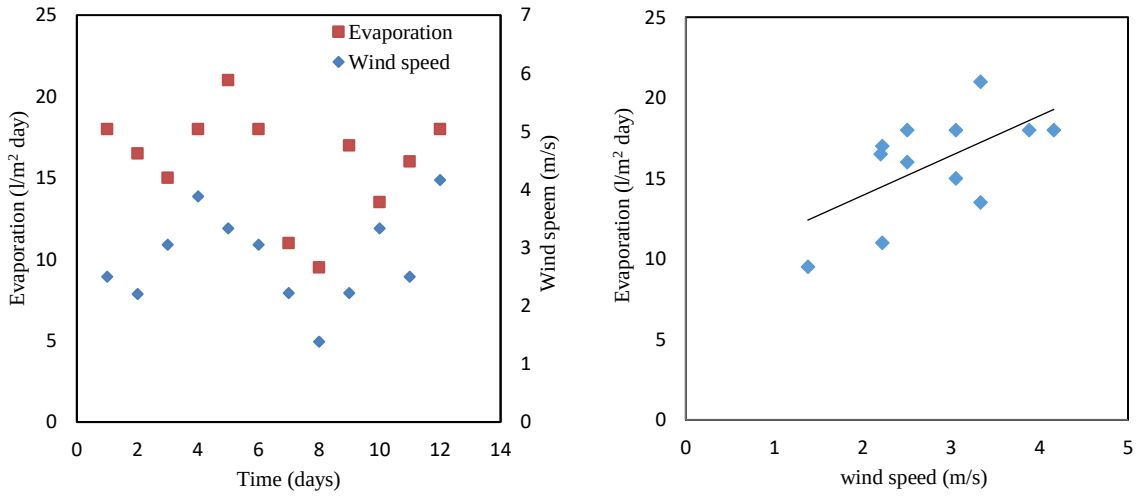

(a) (b)

Figure 3: (a) Daily average measurements of evaporation rate and wind speed above the pond for 12 days from 29/7-9/8/2015, (b) Scatter plot of evaporation rate against wind speed

Figure 3(a) illustrates that during the 12 days, wind speed may have influenced evaporation: evaporation increased in line with increasing wind speed, and fluctuated similarly. Figure 3(b) illustrates that during the 12 days considered; there is a strong positive correlation between wind speed and the evaporation rate (R = 0.6). However, it is less marked than that for relative humidity (R = -0.85) and similar in magnitude to that of the ambient temperature (R = -0.59).

These results are for a short-term study (12 days) which is clearly insufficient to establish a clear understanding of the effects of the various climatic factors on the evaporation rate. Therefore, the meteorological measurements from Nasiriyah City's meteorological station were considered for a long-term study (nine months, January to September) to build up a clearer picture.

Firstly, results from the 12 days before the paraffin addition were compared with the measurements of the Nasiriyah meteorological station. The differences between the ambient temperature and relative humidity measured in the present study and recorded at the meteorological station are not significant. Differences in the measured ambient temperatures (about 1.5 °C) might be because the experimental SGSP site was about 5 km from the meteorological station. A similar explanation could account for the difference in the relative humidity (variation around 1% in relative humidity). Nevertheless, the agreement is acceptable. Interestingly, the evaporation rates in the present study were predominantly lower than the meteorological measurements. This discrepancy could result from the variation in salinity of the two sources used for measurement: the meteorological measurements used fresh water, while in the present study; the water which evaporated from the pond surface had a non-zero

salt concentration due to the upward diffusion of salt from the bottom of the pond. This concentration changed daily as a result of the continuous diffusion. Finch and Hall (2001) implied that the evaporation rate decreases by approximately 1% for each 1% increase in the salt concentration. This is because the vapour pressure of the saline water will drop. Torkmahalleh et al. (2017) concluded that increases in ambient temperature affected the evaporation rate from the UCZ and also increased the salt diffusion rate. They recommended regular surface washing to preserve the concentration of the UCZ at the normal level, and consequently protect the stability of the pond.

According to the meteorological measurements, the rate of water losses increased from March (≈5.35 l/m^2 day) and reached its highest value in June (≈ 17.68 l/m^2 day). After June, there was a small decrease to reach ≈ 11.78 l/m^2 day in September. These levels are significant: for example, if a pond has a surface area of 1,000 m^2, 5,350 litres of fresh water would be needed each day in March to replenish the UCZ; and in June, July and August, around 17,000 l/day would be required. These amounts might decrease by 10-15% because of the effect of the salinity of the UCZ. If the pond were to be used for desalination, this could have a significant impact on the production rate, and hence the economics of the operation. Ruskowitz et al. (2014) implied that when a solar pond is used for fresh water production in locations with a shortage of fresh or clean water, suppressing surface evaporation is entirely worthy. They based their conclusions on the fact that in some previous studies (e.g. Walton et al., 2004; and Solis, 1999), where the aim was to study fresh water production from a membrane distillation system coupled with a SGSP, it was observed that the volume of water produced was less than the volume that evaporated from the surface of the pond. Therefore, to replenish the UCZ, fresh or clean water is required in large quantities - somewhat negating the need for desalination in the first place!

The monthly average relative humidity, ambient temperature and evaporation levels at the Nasiriyah weather station for nine months are plotted against time in Figure 4.

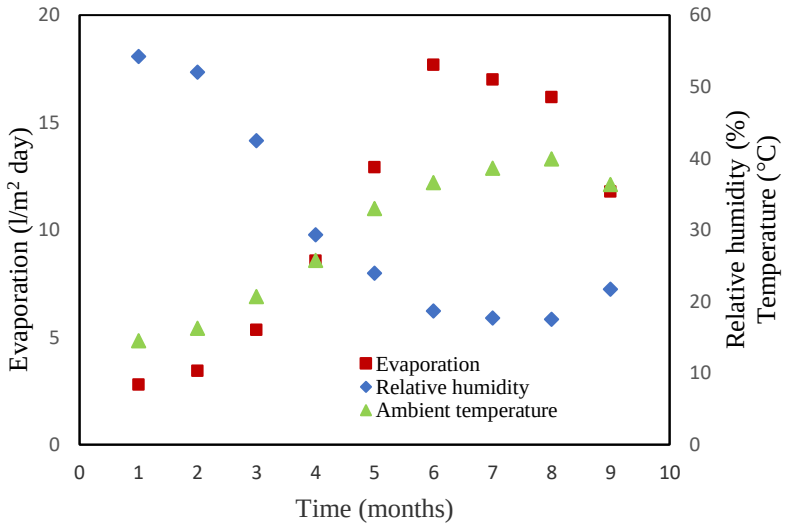

(a)

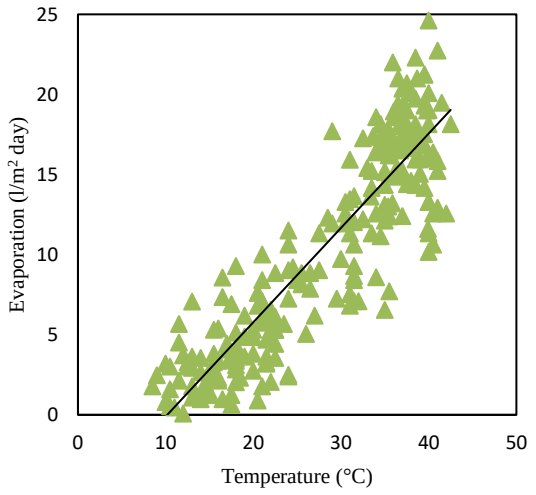

(b)

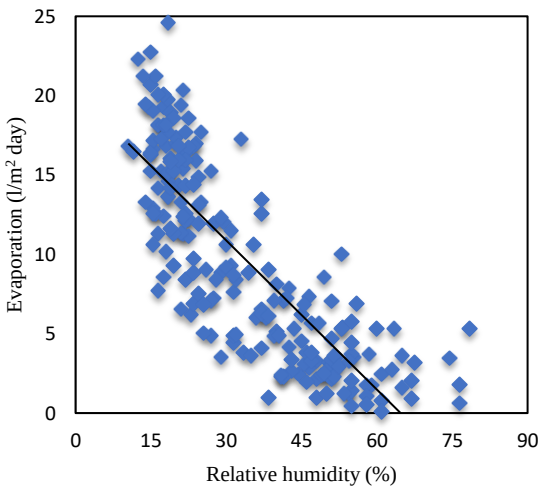

(c)

Figure 4: (a) Monthly average relative humidity, ambient temperature and evaporation levels plotted against time, where month 1 is January, (b) Daily measurements of evaporation rate plotted against ambient temperature, (c) Daily evaporation rate plotted against relative humidity

Using the long-term measurements in Figure 4(a), a notable correlation can be seen between the evaporation rate and the ambient temperature. Moreover, the daily measurements in Figure 4(b) demonstrate that the temperature in the long-term investigation has a strong correlation with the evaporation rate. The correlation coefficient of the measurements of Figure 4(b) is R = 0.88, and is higher than that for the short-term data (R = -0.59). This high value (0.88) illustrates that there is a strong correlation. Figure 4(a) shows that the evaporation rate rose as the ambient temperature increased for the first five months, from January to May. From

May to August the increase in the ambient temperature was small (≈ 5 °C). However, the increase in evaporation levels continued, with a maximum being reached in June. While the ambient temperature increased from May to reach a maximum in August, there was a moderate decrease in the evaporation rate from June to August. That behaviour clarifies that the other factors (humidity, solar radiation and wind speed) might also affect the evaporation.

The measured relative humidity shows that the highest value was in January (around 54 %), and after that, it decreased to reach the lowest value in August (about 17.5%). After August the relative humidity increased again. The evaporation rate appeared to vary inversely with relative humidity: while relative humidity decreased from January, evaporation increased and reached its maximum rate in June. Interestingly, when the fluctuation in relative humidity was small (during June, July and August), there was little variation in the evaporation levels. Figure 4(a) illustrates that evaporation reduced significantly with high relative humidity. It is also apparent from Figure 4(c) (R = -0.83) that the highest evaporation levels occur with the lowest values of relative humidity. This is consistent with physical intuition.

The effect of wind speed was also studied over the longer time period. The dependence of the evaporation rate on wind speed is shown in Figure 5.

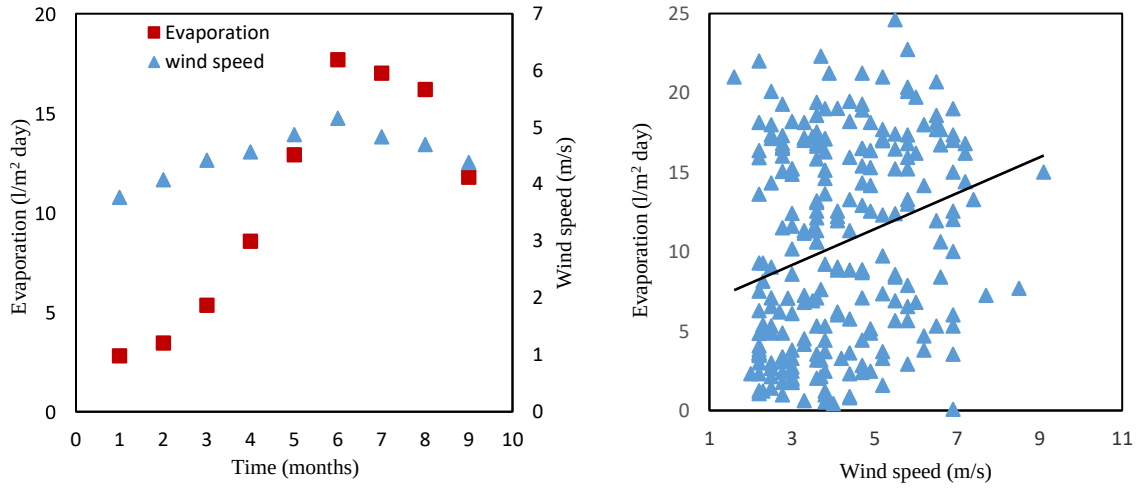

(a) (b)

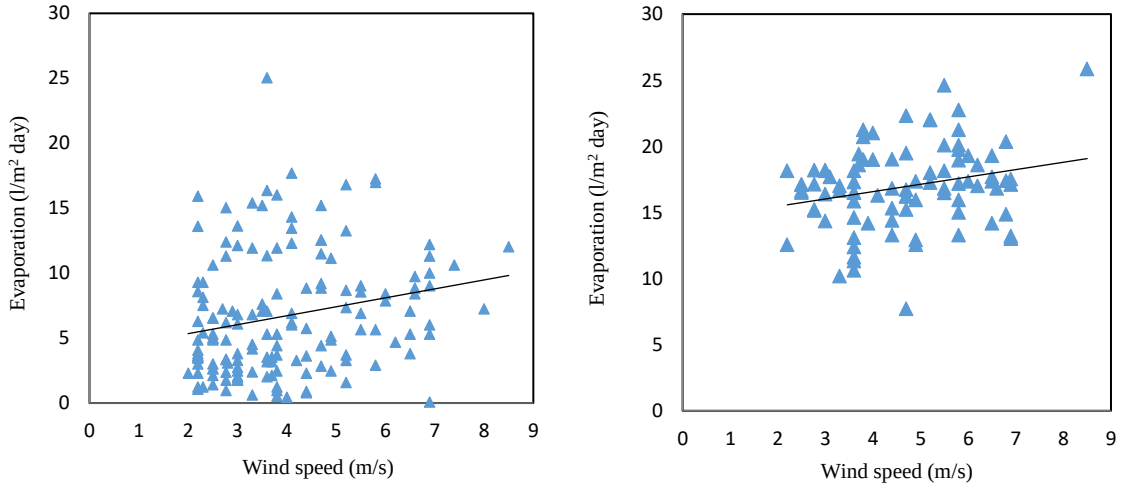

(c) (d)

Figure 5: (a) Measurements of monthly average evaporation rate and wind speed against time over nine months (January-September, month 1 is January), (b) Daily measurements of evaporation plotted against wind speed for the nine-month period, (c) Daily measurements of evaporation plotted against wind speed for January to May, and (d) Daily measurements of evaporation plotted against wind speed for June to September

During the 9 months considered, the average monthly wind speed varied between ≈ 3.7 to ≈ 5.1 m/s, and the maximum speed was in June. The wind speed throughout the period increased slightly from winter toward summer. With the relatively small increase in the wind speed over time, there was a substantial increase in the evaporation rate. From April to June, in spite of the average wind speed increasing only a little (from 4.5 to 5.1 m/s), there was a considerable increase in the evaporation rate, which reaches its maximum level in June (from 8.56 to 17.68 l/m^2 day). From June to September, Figure 5a shows that the evaporation rate decreases, as does the average wind speed. Figure 5b (all daily measurements) shows that for the whole period (9 months), there is only a weak correlation between the wind speed and the evaporation. The points are somewhat scattered in a wide band and the correlation coefficient R = 0.26. Results in Figure 5b contradict the results of the short-term study (Figure 3b, where the correlation coefficient is 0.6). Figure 5b can be divided into two parts. The first where there is a weaker correlation between wind speed and evaporation (from January until the end of May); this period is illustrated in Figure 5c. The second part, where there is a slightly stronger correlation, runs from June to the end of September and is shown in Figure 5d. Obviously, wind speed has a lesser influence on the evaporation from the surface in the colder weather. However, its impact is more significant in the warm and hot weather (from May to September in Figure 5a).

The final climatic factor, which can affect the evaporative losses from the pond is the incident solar radiation. This was not measured in the short-term study. For the long-term study,

the measurements of radiation from NASA (2014) have been considered to study the effect of this factor on the evaporation from the surface of the pond. Results are shown in Figure 6.

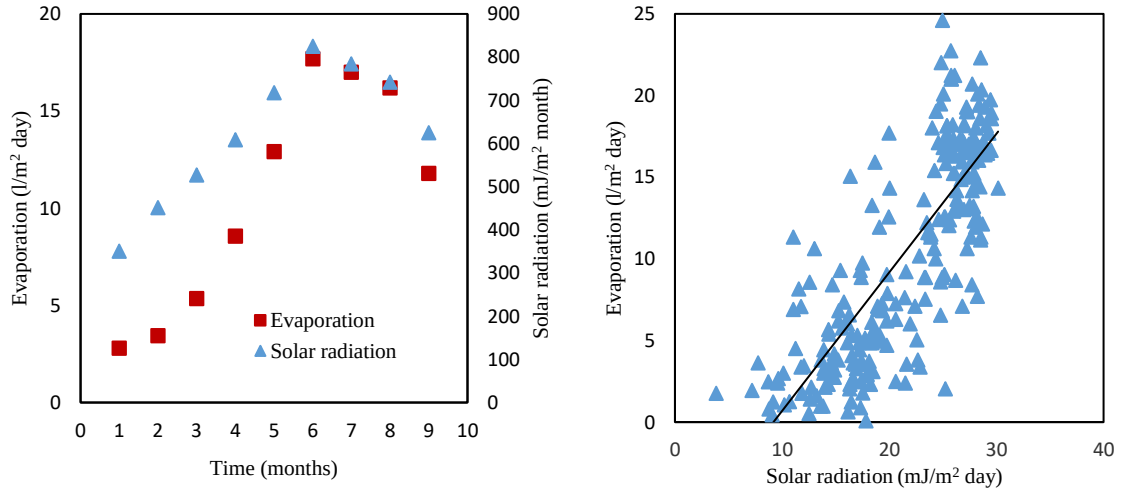

(a) (b)

Figure 6:(a) Measurements of monthly average evaporation levels and incident solar radiation against time, (b) Evaporation rate plotted against solar radiation for each day of the nine months

As radiation increased almost linearly from January to June, there was also an increase in the evaporation rate. Noticeably, the incident solar radiation and evaporation attained their maximum in June. From June, both the evaporation rate and incident radiation decreased, reaching their lowest magnitudes in September. It is apparent from Figure 6(a) that incident radiation might have an important effect on evaporation. This factor, which ultimately drives the pond, does not therefore come without an associated cost in the form of increased evaporative losses. Figure 6(a) shows a significant correlation between solar radiation and evaporation, while Figure 6(b), showing daily measurements, has a weaker correlation than the ambient temperature. It can be seen in Figure 6(b) that the reliance of daily evaporation on solar radiation might be lower than the reliance on temperature and relative humidity. The correlation coefficient is 0.80: it shows a significant relationship but not as strong as the other climatic factors (ambient temperature 0.88 and relative humidity -0.83).

To find a relationship which can gather all climatic factors together with the evaporation, a statistical analysis was performed on the extended period measurements to predict this relationship. Table 1 gives some statistics which were generated using a multiple regression analysis (in the present investigation, only the linear term is considered, and interaction effects are neglected).

Table 1: Statistical data of multiple regression analysis

R^2= 0.81156, adjusted R^2 = 0.80838				
	Coefficients	*Standard Error*	*t Stat*	*P-value*
Intercept	-1.2234	1.882396	-0.64992	0.516375
Solar radiation	0.106939	0.059791	1.788545	0.074965
Ambient temperature	0.380862	0.045975	8.284036	8.81E-15
Relative humidity	-9.31657	2.287592	-4.07265	6.34E-05
Wind speed	0.412576	0.123479	3.341269	0.000969

As usual, R^2 represents the deviation of measured data from the fitted or predicted model or equation. It is expected that the value of R^2 should increase when a new variable is added to the analysis. However, this increase in R^2 does not mean that the accuracy increases. The adjusted R^2 is more accurate than R^2 because it considers values of R^2 and the number of variables in addition to the number of the observations. It is represented as:

$$AdjR^2 = 1 - (1 - R^2)\frac{n-1}{n-k-1} \qquad (1)$$

where n is the number of observations and k is the number of variables. If a useful variable is added to the statistical analysis, the value of the adjusted R^2 will increase. However, if the added variable is insignificant, there will be no improvement in the adjusted R^2. When this occurs, the variable can be excluded from the suggested model or equation.

Table 1 shows that all of the climatic factors have a statistically significant impact on the model ($p < 0.001$) except solar radiation, which is not significant even at $p < 0.05$. The model generated by the regression analysis, including all four variables, has R^2= 0.81156 and $AdjR^2$ = 0.80838 and that means an average error of about 20% is expected.

If the solar radiation is excluded and the regression analysis performed again, the results shown in Table 2 are achieved.

Table 2: Statistical data of multiple regression analysis (excluding incident solar radiation)

R^2= 0.809017, adjusted R^2= 0. 0.80661				
	Coefficients	*Standard Error*	*t Stat*	*P-value*
Intercept	-0.146	1.791627	-0.08149	0.935118
Ambient temperature	0.42634	0.03848	11.07939	2.81E-23
Relative humidity	-10.0035	2.265518	-4.41553	1.53E-05

Wind speed	0.45441	0.121802	3.730722	0.000239

Interestingly, there is only a slight reduction in the values of both R^2 and $AdjR^2$. It might be solar radiation can be excluded from the fitted model.

3.2 Temperature evolution in the pond

3.2.1 Behaviour before coverage

After construction, the pond was ready to collect and store solar insolation. For the first 12 days it was left uncovered. The temporal temperature developments in the UCZ and LCZ, as well as the ambient temperature, are shown in Figures 7(a) and (b) at 2 pm and 2 am local time respectively.

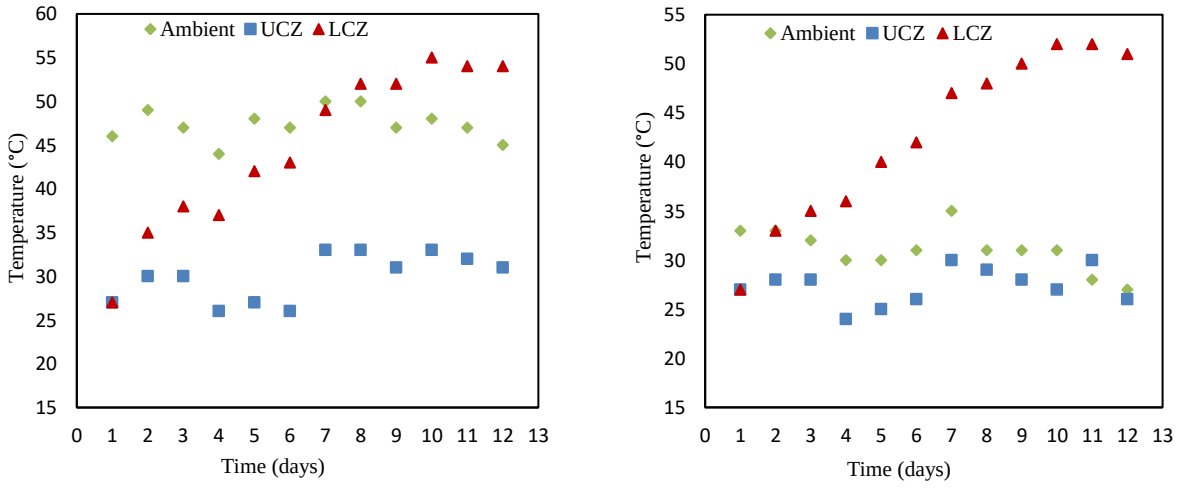

Figure 7: (a) Evolution of daytime temperature (2 p.m.) in UCZ, LCZ and ambient temperature over the first 12 days of operation (29/7-9/8/2015), (b) Evolution of night-time temperature (2 a. m.) in the UCZ, LCZ and ambient temperature over the first 12 days of operation (29/7-9/8/2015)

The results show that the temperature in the LCZ increased from ≈ 27 °C on the first day to around 54 °C on Day 12 with an average rate of increase about 2.25 °C/day, as shown in Figure 7(a). On Day 12 the difference between temperatures in the LCZ and UCZ was around 23 °C during the daytime and 25 °C at night. Figures 7(a) and (b) illustrate that the gap between the ambient and UCZ temperatures is large in the day, but smaller at night. This behaviour could be a result of two facts. Firstly, in the daytime, ambient temperatures throughout the 12 days were high (around 47 °C), falling at night to around 30 °C. Secondly, the evaporation rate is high in the day due to the presence of the solar radiation, low relative humidity, high

temperatures and hot wind. Evaporating water will remove the latent heat from the water in the UCZ, and that will result in a decrease in its temperature.

The temperature variation at different depths in the daytime is illustrated in Figure 8 for Days 2, 6 and 12, i.e. before the pond was covered.

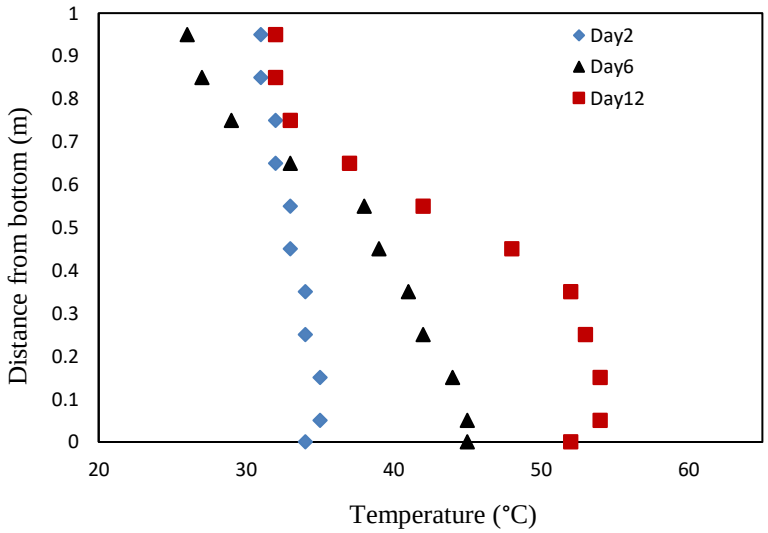

Figure 8: Temperature variation with depth for Days 2, 6 and 12, measured at 2 p.m.

It is clear from Figure 8 that the temperature gradient in the NCZ increased and that there was also an increase in the difference between the temperatures of the LCZ and UCZ. This difference was about 3 °C on the second day, rising to ≈ 19 °C on Day 6 and ≈ 23 °C on Day 12. It is clear that after 12 days, the three zones in the pond have become established, with an approximately uniform temperature in the LCZ, the 40 cm layer at the bottom of the pond. There is also an almost linear variation in temperature over the next 50 cm of depth corresponding to the NCZ, and then a uniform temperature in the top 10 cm where the UCZ is again well-mixed.

3.2.2 Behaviour after pond coverage

After 12 days, and once it was clear that the three layers of the pond had become established, the pond was covered by the thin paraffin layer to eliminate the effect of evaporation. The behaviour of each zone is considered, in turn, below. The temperature profiles both during the day and at night are considered. For completeness, and to aid understanding, the temperature profiles before coverage have also been included.

3.2.2.1 The UCZ

The profiles of the UCZ and ambient temperature are shown in Figures 9(a) and (b) for the daytime (2 p. m) and night-time (2 a. m) through the study.

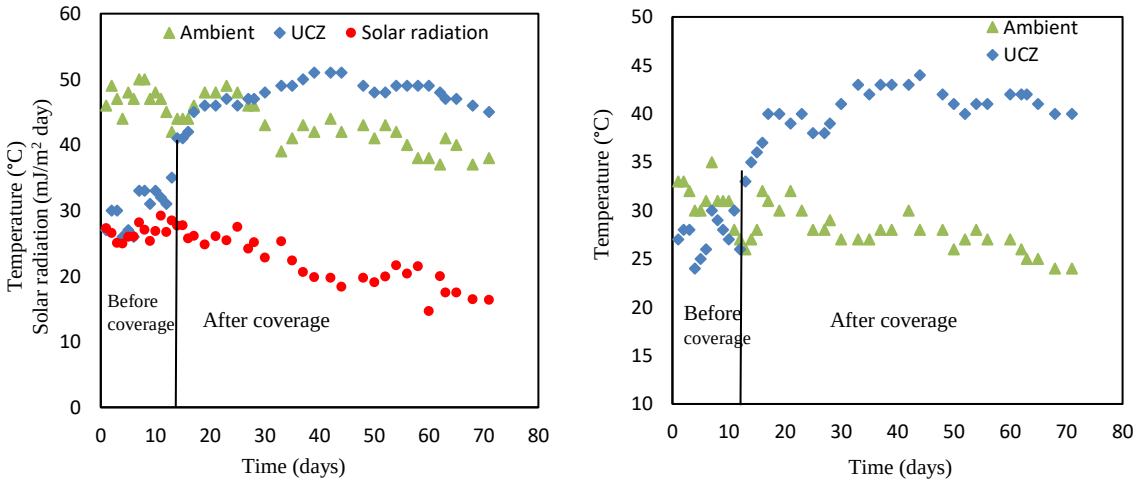

(a) (b)

Figure 9: (a) Measurements of the UCZ, ambient temperature and solar radiation from 29/7-7/10/2015 (daytime 2 p. m), (b) Measurements of the UCZ and ambient temperature from 29/7-7/10/2015 (night-time 2 a. m)

Figures 9(a) and 7(a) (for the uncovered pond) show that in the first 12 days, when the pond was uncovered, the temperature of the UCZ was lower than the ambient temperature and its variation was similar to that of the ambient temperature. Figure 9(a) demonstrates that the trend of both temperatures is approximately similar to that of solar radiation. These results agree with the findings of Torkmahalleh et al. (2017), who found that when the pond is uncovered, the UCZ and ambient temperatures have similar trends and they mostly affected by the solar radiation. This behaviour is because the UCZ receives heat from the LCZ by conduction, and some of the incident solar radiation accumulates in this layer. However, the layer also loses heat to the atmosphere by radiation, convection and evaporation. Moreover, it also loses heat through the pond walls, although this loss is very small and can be neglected when the walls are well insulated. Due to heat loss, the temperature in the UCZ tended to be lower than the ambient air in the daytime during the current study, and the gap between the two temperatures was relatively large (before pond coverage). This behaviour has also been observed by many other researchers e.g. Garman and Muntasser (2008); Al-Jamal and Khashan (1996); and Jaefarzadeh and Akbarzadeh (2002).

After the addition of the paraffin layer, the evaporation process was stopped or significantly reduced. There was no further drop in the water level, so no additional water was required for the remainder of the study. This is obviously a significant operational improvement. Figure 9(a) illustrates that the daytime temperature of the UCZ increased significantly to reach a maximum of 51 °C after about a month. Then there was a small decrease in the UCZ temperature to ≈ 47 °C from the middle of September 2015 to the end of the study. The figure shows also that although there was a decrease in the incident solar radiation, there was an increase in the UCZ temperature. As evaporation has been shown to be the dominant mode of heat loss, most of the heat entering will now be trapped by the paraffin layer, heat will accumulate, and the temperature will increase. In other words, suppressing evaporation significantly increases the UCZ temperature. Figure 9(a) shows that the evolution of the UCZ temperature is different from the ambient temperature's behaviour. While there was a daily fluctuation in the ambient temperature, only a very slight variation can be observed in the profile of the UCZ. Moreover, the gap between the two temperatures in the daytime is relatively small.

From Figures 9(b) and 7(b), relating to the uncovered pond, it can be observed that the night-time UCZ temperature was lower than the ambient temperature; it also behaved similarly to the ambient temperature, with similar variations. On the other hand, the gap between the two temperatures was much smaller than in the daytime. After the pond coverage (i.e. when there is no evaporation), the UCZ temperature rose above the ambient temperature, as seen in Figure 9(b), and the gap between the two temperatures was bigger than in the daytime. While the ambient temperature decreased noticeably in the night, the reduction in the UCZ temperature was insignificant, due to heat accumulation from the LCZ. The night-time UCZ temperature reached a maximum of around 44 °C, and then decreased to ≈ 37 - 39 °C until the end of the study. Apparently, the UCZ became in effect a new storage zone in which heat accumulated to a much greater degree than in the uncovered pond. This is clearly demonstrated by the fact that its temperature reached 51 °C and remained approximately constant with only a very gentle decline to ≈ 47 °C (daytime) over a period of about 20 days. Date and Akbarzadeh (2013) suggest that around 45% of the incident solar radiation is absorbed in the UCZ of a traditional SGSP, but is lost again to the atmosphere. Sayer et al. (2016) concluded that heat loss from the pond's surface is mainly due to evaporation. With the new approach (covered pond), most of the heat which is absorbed or transferred from the LCZ through the NCZ and accumulated in

the UCZ can be exploited, since heat loss to the atmosphere becomes relatively small with evaporation suppression.

3.2.2.2 The LCZ

The profiles of the LCZ, UCZ and ambient temperature are illustrated in Figure 10.

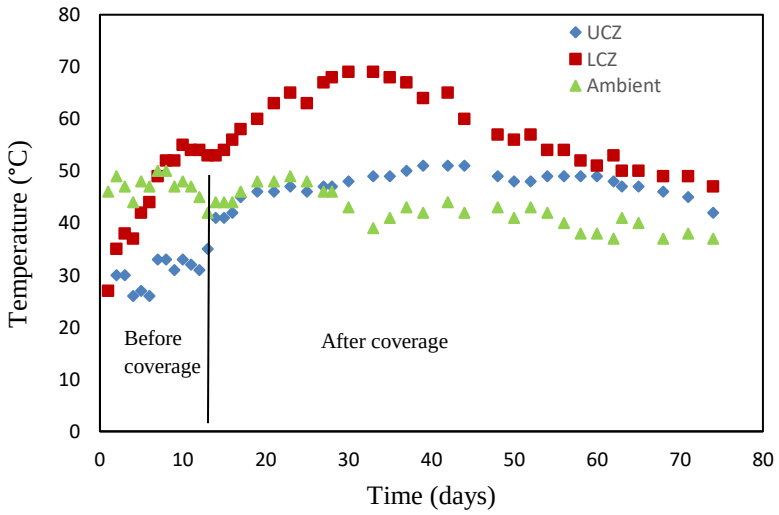

Figure 10: Change in LCZ, UCZ and ambient temperature in daytime (2 p m) from 29/7-7/10/2015

In the first 12 days before adding the cover, the rate of increase in the temperature of the LCZ was relatively fast, at around 2.25 °C/day. However, when the pond was covered, the rate of increase became slightly lower. It was observed that dust accumulated on the surface of the paraffin layer, thereby attenuating the incoming radiation. After the pond was covered, the rate of the temperature increase reduced to 1.25 °C/day, for the period from Day 12 to Day 30. The LCZ temperature reached its maximum (69 °C) on Day 30 - about 17 days after the paraffin addition. After the maximum temperature in the LCZ was attained at the end of August, there was a gradual decrease to ≈ 50 °C during the last period of the study. Figure 10 illustrates that when the pond was open to the atmosphere, the gap between the temperatures of the LCZ and UCZ was relatively large. This gap became smaller and smaller from the beginning of September to the end of the present study. The reduction in the gap between the two temperatures might be due to the decline in the incident solar radiation as shown in Figure 9(a), and the increase in UCZ temperature caused by evaporation suppression. This behaviour is different from that of the open pond. For example, Torkmahalleh et al. (2017) found that the difference between the temperatures of the layers follows the solar energy intensity, but the trend of the temperature follows that of the ambient temperature. In the final few days of the

current study, the difference between the two temperatures was small. Figure 10 also shows that before the pond was covered, the LCZ temperature fluctuated slightly in an identical way to the ambient temperature. After coverage, the LCZ fluctuation was significantly different from the ambient temperature variation.

3.2.2.3 Temperature variation with depth

The change in temperature profile within the pond, before and after the pond was covered, is shown in Figure 11.

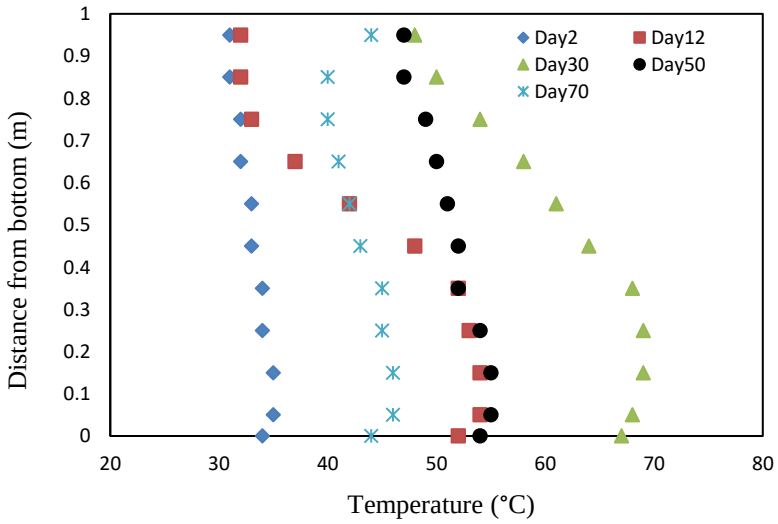

Figure 11: Temperature distribution in the experimental pond on different days before and after coverage

Many interesting features can be identified in Figure 11. Firstly, after the pond was covered, the LCZ temperature continued to increase, reaching its maximum of 69 °C on Day 30, after which it decreased. Interestingly, there was also an increase in the UCZ temperature, and the difference between the two temperatures on Day 30 was ≈ 21 °C. Normally, when the LCZ reaches the maximum temperature, the temperatures of the UCZ also reaches the maximum, and they both behave similarly to the ambient temperature (Torkmahalleh et al., 2017; Sayer et al., 2016; Jaefarzadeh and Akbarzadeh, 2002). Torkmahalleh et al. (2017) observed that in an uncovered SGSP, the LCZ and UCZ temperatures were affected by the ambient temperature and incident solar radiation, and mainly followed the behaviour of the ambient temperature. In a pond where evaporation is suppressed, the behaviour is significantly different. As previously discussed, it might be that the dust which accumulated on the surface decreased the quantity of solar radiation reaching the LCZ and consequently decreased its temperature.

Secondly, it is also interesting to note that on Day 30, there was an apparent and uniform temperature gradient through the NCZ. As time progressed, however, this gradient diminished

substantially. This might be due to the accumulation of heat in the UCZ, which will thus raise its temperature. The disruption of the temperature gradients could be thought to be indicative of the destruction of the salinity gradient, and hence the pond becoming well-mixed. However, concentration measurements indicated that there were salinity gradients in the NCZ (Figure 12), and that in spite of these, there was a significant decrease in the temperature gradients. This would support the hypothesis that it is not convective heat transfer that has made the temperature profile uniform; rather it is a conductive effect.

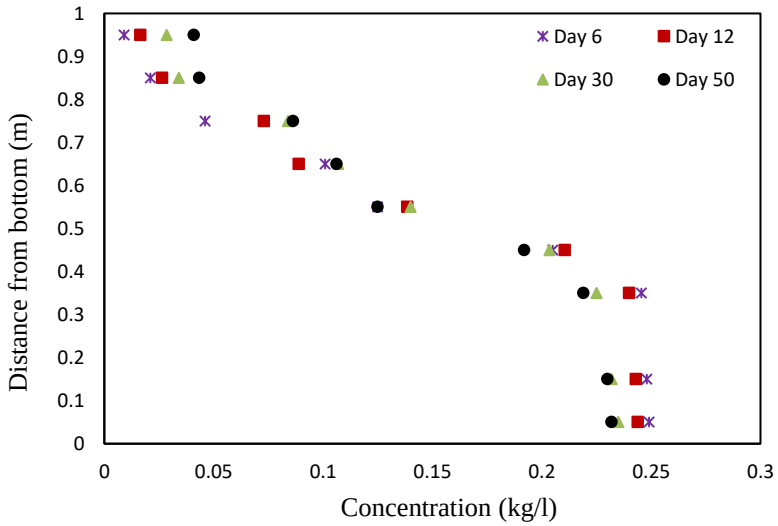

Figure 12: Salinity gradient of the experimental pond on different days before and after covering

Figure 12 shows apparent salinity gradients on the chosen days. For example, at Day 50, the gradient remains intact with a relatively substantial increase in the salinity of the UCZ, but the temperature gradient on that day (Figure 11) is small. It is worth noting that as shown in Figure 12 Day 50, the concentration of the UCZ is close to the concentration of the top layer of the NCZ. This means that surface washing of the LCZ has to be carried out immediately to avoid erosion in the top layer of the NCZ.

Thirdly, it is important to note that in the conventional SGSP, the UCZ temperature changes from high to low magnitude when moving from summer to winter and *vice versa*. In this pond, there was an increase towards winter to reach the maximum and then a small decrease was observed.

4. Conclusion

The aim of this study was to investigate the behaviour of a salinity gradient solar pond (SGSP) with and without a thin liquid paraffin cover to suppress evaporation from the surface of the

pond. A small SGSP was constructed with a 1 m^2 surface area and a depth of 1 m. The UCZ, NCZ and LCZ were 0.1, 0.5 and 0.4 m deep respectively, while the paraffin cover had a thickness of 0.5 cm. The effect of different climatic factors (relative humidity, ambient temperatures wind speed and solar radiation) on evaporation was also investigated. It was observed that evaporation was entirely eliminated by the paraffin layer.

The results clearly highlight that suppressing evaporation is highly beneficial to the pond's performance, significantly reducing the cost of water replacement and thus making applications such as desalination more economically viable. This study therefore provides the initial verification that a non-volatile liquid cover can significantly affect and improve the thermal performance of a solar pond. The research also highlights a number of issues that must be addressed going forward. The paraffin layer accumulated dust much more readily than the uncovered pond and this could attenuate the incoming radiation. Furthermore, the effect of wind (and hence surface waves) and rain on the stability of the surface layer must be investigated. Finally, this proof-of-concept study used paraffin as the covering fluid as it could be guaranteed to supress evaporation. It is however not without associated environmental concerns. Given the success in trapping more heat in the pond, the investigation of alternative covering fluids must now be considered.

References

Abbassi Monjezi, A., Campbell, A. N., 2016. A comprehensive transient model for the prediction of the temperature distribution in a solar pond under Mediterranean conditions. Sol. Energy 135, 297–307.

Abbassi Monjezi, A., Campbell, A. N., 2017a. A comparative study of the performance of solar ponds under Middle Eastern and Mediterranean conditions with batch and continuous heat extraction. Applied Thermal Engineering 120, 728–740.

Abbassi Monjezi, A., Mahood, H.B., Campbell, A.N., 2017b. Regeneration of dimethyl ether as a draw solute in forward osmosis by utilising thermal energy from a solar pond. Desalination (accepted manuscript). DOI: 10.1016/j.desal.2017.03.034

Abdullah, A. A., Lindsay, K. A., AbdelGawad, A. F., 2016. Construction of sustainable heat extraction system and a new scheme of temperature measurement in an experimental solar pond for performance enhancement. Sol. Energy 130, 10–24.

641 Abdullah, A. A., Lindsay, K. A., AbdelGawad, A. F., 2015. Parsimonious constitutive
642 expressions with good accuracy and suitable for modelling the properties of aqueous sodium
643 chloride in solar ponds. Sol. Energy 122, 617–629.
644 Abdullah, A. A., Lindsay, K. A., 2016. Solar Ponds: Some issues in their management and
645 mathematical description. Twelfth international conference of fluid dynamics (ICFD12), 19-
646 20 December, Le Méridien Pyramids Hotel, Cairo, Egypt, ICFD12-EG-5038.
647 Aizaz, A., Yousaf, R., 2013. Construction and analysis of a salt gradient solar pond for hot
648 water supply. European Scientific journal 9, (36).
649 Akbarzadeh, A., Ahmadi, G., 1979. Underground thermal storage in the operation of solar
650 pond. Energy 4, 119–1125.
651 Akbarzadeh, A., Andrews, J., Golding, P. 2005. Solar Pond Technologies: A review and Future
652 Directions. Advances in Solar Energy. Earthscan. London, UK, 16, 233–294.
653 Alagao, F. B., Akbarzadeh, A., Johnson, P., 1994. The design, construction, and initial
654 operation of closed-cycle salt gradient solar pond. Sol. Energy 53, 343–351.
655 Alagao, F. B., 1996. Simulation of the transient behaviour of a closed-cycle salt- gradient solar
656 pond. Sol. Energy 56 (3), 245–260.
657 Ali, H. M., 1989. Potential of solar ponds in hot climates. Solar & Wind Technology 6 (2),
658 137–141.
659 AL-Jamal, K., Khashan, S., 1998. Effect of energy extraction on solar pond performance.
660 Energy Convers. Mgmt. 39 (7), 559–566.
661 Alrowaished, A., Azni, I., Mohamed, T. A., Amimul, A., 2013. The development and
662 applications of solar pond: a review. Desalination & Water Treatment 10, 1–13.
663 Antipova, E., Boer, D., Cabeza, L. F., Gosalbez, G. G., Jimenez, L., 2013. Multi-objective
664 design of reverse osmosis plants integrated with solar Rankine cycles and thermal energy
665 storage. Applied Energy 102, 1137–1147.
666 Assari, M. R., Tabrizi, H. B., Nejad, A. K., Parvar, M., 2015. Experimental investigation of
667 heat absorption of different solar pond shapes covered with glazing plastic. Sol. Energy 122,
668 569–578.
669 Assouline, S., Narkis, K., Or, D., 2010. Evaporation from partially covered water surfaces.
670 Water Resources Research 46, W10539. http:// dx.doi.org/10.1029/2010WR009121.
671 Bozkurt, I., Karakilcik, M., 2012. The daily performance of a solar pond integrated with solar
672 collectors. Sol. Energy 86, 1611–1620.
673 Caruso, A., Navigilio, A., 1999. Desalination plant using solar heat as a heat supply, not
674 affecting the environment with chemicals. Desalination 122, 225–234.

675 Dah, M. M., Ouni, M., Guizani, A., Belghith, A., 2010. The influence of the heat extraction
676 mode on the performance and stability of a mini solar pond. Applied Energy 87, 3005–3010.
677 Date, A., Akbarzadeh, A.,2013. Salinity gradient solar ponds. In: Napoleon, E., Akbarzadeh,
678 A. (Eds.) Energy Sciences and Engineering Applications. CRC press. E. Book.
679 Dehghan, A. A., Movahedi, A., Mazidi, M., 2013. Experimental investigation of energy and
680 energy performance of square and circular solar ponds. Solar energy 97, 273-284.
681 El-Sebaii, A. A., Ramadan, M. R. I., Aboul-Enein, S., Khallaf, A. M., 2011. History of the
682 solar ponds: a review study. Renewable and Sustainable Energy Reviews 15, 3319–3325.
683 Finch, J. W., Hall, R. L., 2011. R & D Technical Report W6-043/TR, www.environment-
684 agency.gov.uk.
685 Garman, M. A., Muntasser, M. A., 2008. Sizing and thermal study of salinity gradient solar
686 ponds connecting with MED desalination unit. Desalination 222, 689–695.
687 Ghaffour, N., Lattemann, S., Missimer, T., Kim, C. N., Sinha, S., Amy, G., 2014. Renewable
688 energy -driven innovative energy-efficient desalination technologies. Applied Energy 136,
689 1155–1165.
690 Gude, V. G., 2015. Energy storage for desalination processes powered by renewable energy
691 and waste heat sources. Applied Energy 137, 877–898.
692 Gude, V. G., Nirmalakhandan, N., Deng, S., Maganti, A., 2012. Low temperature desalination
693 using solar collectors augmented by thermal energy storage. Applied Energy 91, 466–474.
694 Hull, J. R., Nielsen, C. E., Golding, P., 1988. Salinity Gradient Solar Ponds. Florida: CRC
695 Press.
696 Husain, M., Sharma, G., Samdarshi, S. K., 2012. Innovative design of non-convective zone of
697 salt gradient solar pond for optimum thermal performance and stability. Applied Energy 93,
698 357–363.
699 Jaefarzadeh, M. R., 2004. Thermal behaviour of a small salinity-gradient solar pond with wall
700 shading effect. Sol. Energy 77, 281–290
701 Jaefarzadeh, M. R., Akbarzadeh, A., 2002. Towards the design of low maintenance salinity
702 gradient solar pond. Sol. Energy 73 (5), 375–384
703 Jahani, E., Sadati, S. M., Yousefzadeh, M., T., Güneş, M., Sarıciftci, S., Varlıklı, C., 2015.
704 Assessment of solar data estimation models for four cities in Iran. Physica Status Solidi (c),
705 12(9-11), 1272-1275.
706 Karakilcik, M., Kiymac, K., Dincer, I., 2006. Experimental and theoretical temperature
707 distributions in a solar pond. International Journal of Heat and Mass Transfer 49, 825–835.

Karakilcik, M., Dincer, I., Bozkurt, I., Atiz, A., 2013. Performance assessment of a solar pond with and without shading effect. Energy Conversion and Management 65, 98–107.

Kishore, V. V. N., Veena, J., 1984. A practical collector efficiency equation for non-convecting solar ponds. Sol. Energy 33 (5), 391–395.

Kurt, H., Halici, F., Binark, A. K., 2000. Solar pond conception - experimental and theoretical Studies. Energy Conversion and Management 41, 939–951.

Leblanc, J., Akbarzadeh, A., Andrews, J., Huanmin, Lu., Golding, P., 2011. Heat extraction methods from salinity–gradient solar ponds and introduction of a novel system of heat extraction for improved efficiency. Sol. Energy 85, 3103–3142.

Liu, X., Caoa, G., Shena, S., Gua, M., Li, C. 2013. The research on thermal and economic performance of solar desalination system with salinity-gradient solar pond. Desalination and Water Treatment 51, 3735–3742.

Nakoa, K., Rahaoui, K., Date, A., Akbarzadeh, A., 2015. An experimental review on coupling of solar pond with membrane distillation. Sol. Energy 119, 319–331.

Rahimi, R., Saadati, S., & Honarvar Fard, E. (2015). Fluorine-doped TiO2 nanoparticles sensitized by tetra(4-carboxyphenyl)porphyrin and zinc tetra(4-carboxyphenyl)porphyrin: Preparation, characterization, and evaluation of photocatalytic activity. Environmental Progress & Sustainable Energy, 34(5), 1341-1348.

Ranjan, K. R., Kaushik, S. C., 2014. Thermodynamic and economic feasibility of solar ponds for various thermal applications: A comprehensive review. Renewable and Sustainable Energy Reviews 32, 123–139.

Ruskowitz, J. A., Suarez, F., Tyler, S. W., Childress, A. E., 2014. Evaporation suppression and solar energy collection in a salt-gradient solar pond. Sol. Energy 99, 36–46.

Salata, F., Coppi, M., 2014. A first approach study on the desalination of sea water using heat transformers powered by solar ponds. Applied Energy 136, 611–618.

Sayer, A. H., Al- Hussaini H., Campbell, A. N., 2016. New theoretical modelling of heat transfer in solar ponds. Sol.Energy 125, 207–218.

Solis, S. S., 1999. Water Desalination by Membrane Distillation Coupled with a Solar Pond. M.Sc. Thesis. ETD Collection for University of Texas, El Paso.

Sakhrieh, A., Al-Salaymeh, A., 2013. Experimental and numerical investigations of salt gradient solar pond under Jordanian climate conditions. Energy Convers and Manage 65, 725–8.

Srinivasan, J., 1993. Solar Pond Technology. Sadhana 18 (1), 39–55.

741 Suarez, F., Ruskowitz, J. A., Childress, A. E., Tyler, S. W., 2014. Understanding the expected
742 performance of large –scale solar ponds from laboratory –scale observations and numerical
743 modelling. Applied Energy 117, 1–10.
744 Suarez, F., Ruskowitz, J. A., Tyler, S. W., Childress, A, E., 2015. Renewable water: Direct
745 contact membrane distillation coupled with solar ponds. Applied Energy 158, 532–539.
746 Surface Meteorology and solar energy, a renewable energy resource web site, available at
747 https://eosweb.larc.nasa.gov (NASA) (accessed on 25 July 2014).
748 Tabor, H., 1980. Non-Convecting Solar Ponds. Philosophical Transactions of the Royal
749 Society of London. Series A, Mathematical and Physical Sciences 295, 423–433. Cited in: Date
750 A, Akbarzadeh A 2013.
751 Torkmahalleh, M. A., Askari, M., Gorjinezhad, S., Eroglu, D., Obaidullah, M., Habib, A. R.,
752 Godelek, S., Kadyrov, S., Kahraman, O., Pakzad, N. Z., Ahmadi, G., 2017. Key factors
753 impacting performance of a salinity gradient solar pond exposed to Mediterranean climate. Sol.
754 Energy 142, 321–329
755 Velmurugan, V., Srithar, K., 2008. Prospects and scopes of solar pond: A detailed review.
756 Renewable and Sustainable Energy Reviews 12, 2253–2263.
757 Walton, J., Lu, H., Turner, C., Solis, S., Hein, H., 2004. Solar and Waste Heat Desalination by
758 Membrane Distillation. Desalination and Water Purification Research and Development
759 Program, UTEP, El Paso.
760 Zaragoza, G., Ruiz, A., Guillen, B. E., 2014. Efficiency in the use of solar thermal energy of
761 small membrane desalination systems for decentralized water production. Applied Energy 130,
762 491–499.
763 Ziapour, B. M., Shokrnia, M., Naseri, M., 2016. Comparatively study between single-phase
764 and two-phase modes of energy extraction in a salinity-gradient solar pond power plant. Energy
765 111, 126–136.
766
767
768
769
770
771